



## Article

# Inversion of Aerosol Particle Size Distribution Using an Improved Stochastic Particle Swarm Optimization Algorithm

Xin Nie <sup>1,2</sup> and Qianjun Mao <sup>1,\*</sup><sup>1</sup> School of Urban Construction, Wuhan University of Science and Technology, Wuhan 430065, China<sup>2</sup> Industrial Safety Engineering Technology Research Center of Hubei Province, Wuhan University of Science and Technology, Wuhan 430081, China

\* Correspondence: maoqianjun@wust.edu.cn; Tel.: +86-27-68893627

**Abstract:** Aerosol particle size distribution (PSD) is one of the main influencing factors of the radiation effects and climate effects of aerosol. An improved stochastic particle swarm optimization (ISPSO) algorithm is proposed, and the PSD characteristics of aerosols were successfully retrieved from the aerosol optical depth (AOD). The performance analysis shows that the algorithm has good global search ability and convergence performance and will not fall into local optima. Then, the robustness and the ability to resist the noise of the algorithm were verified by adding random errors, using random initial values, and changing the number of samples and inversion parameters, and it was shown that the algorithm has a weak dependence on the initial value. The PSD characteristics of three typical aerosols were inverted, and the results show that the algorithm has good adaptability to the inversion of aerosol PSD. Finally, the PSD characteristics of aerosols from Xianghe and Mezaira under typical weather were inverted based on AERONET data, which shows the effectiveness and advancement of the ISPSO algorithm. This study can provide help for the obtaining of aerosol parameters under poor optical conditions.



**Citation:** Nie, X.; Mao, Q. Inversion of Aerosol Particle Size Distribution Using an Improved Stochastic Particle Swarm Optimization Algorithm. *Remote Sens.* **2022**, *14*, 4085. <https://doi.org/10.3390/rs14164085>

Academic Editors: Manuel Antón and Carmine Serio

Received: 4 July 2022

Accepted: 13 August 2022

Published: 20 August 2022

**Publisher's Note:** MDPI stays neutral with regard to jurisdictional claims in published maps and institutional affiliations.



**Copyright:** © 2022 by the authors. Licensee MDPI, Basel, Switzerland. This article is an open access article distributed under the terms and conditions of the Creative Commons Attribution (CC BY) license (<https://creativecommons.org/licenses/by/4.0/>).

**Keywords:** improved stochastic particle swarm optimization; aerosol; particle size distribution; inversion

## 1. Introduction

Atmospheric aerosol is a colloidal system composed of solid and liquid particles and gas in the atmosphere. It is a multiphase mixture with multi-scale characteristics, with diameters ranging from 0.001 to 100  $\mu\text{m}$  [1–3]. Atmospheric aerosol is also the main participating medium of atmospheric radiation. It affects the Earth's energy balance through direct and indirect radiation effects and is one of the biggest sources of uncertainty in the assessment of global climate change [4–6]. Due to the significant spatiotemporal heterogeneity of aerosol and the accompanying uncertainty of optical observations, the accurate inversion of aerosol optical properties has always been a difficult point in the field of atmospheric research and remote sensing [7,8].

Countries worldwide have developed a variety of optical and remote sensing equipment for effectively obtaining the optical property parameters of atmospheric aerosols, including different satellite-based, ground-based, and mobile detectors [9–11]. This equipment provides great help for observation and inversion research on aerosols. However, the existing remote sensing equipment can only obtain the optical properties of aerosols in a finite spectrum. The optical properties in other wavelengths are generally obtained by indirect methods. Specifically, physical parameters such as aerosol particle size distribution (PSD) are obtained by inversion, and then the required aerosol optical properties are calculated by these physical parameters [12–14]. For decades, researchers have developed a large number of techniques and methods to obtain the PSD of aerosols, such as the aerodynamic method, optical method, electrical sensing zone method, electrical mobility method, condensation methods, etc. [15]. Among them, the optical method is

widely used in PSD inversion due to its advantage in obtaining temporal-spatial data, such as the extinction method. For example, Lee et al. developed a new method for inversion of aerosol PSD based on spectral extinction technique and optical depth [16]. He et al. performed a nonparametric estimation of the aerosol PSD using spectral extinction and regularization [17]. Wurl et al. used a nonlinear estimation method to invert the PSD characteristics of small aerosol particles based on multi-wavelength extinction data [18].

In recent years, a large number of numerical algorithms have been used to solve optimization problems such as the inversion of PSD. There are mainly two types that are widely used at present; one is based on the gradient-based techniques, such as the Levenburg–Marquardt method and Gauss–Newton method [19,20], and the other are the heuristic intelligent optimization algorithms, such as the genetic algorithm, ant colony optimization algorithm, fruit fly optimization algorithm, and particle swarm optimization algorithm (PSO) [21,22]. The former algorithm was developed earlier and has been widely used to invert the PSD characteristics of aerosols. For example, Stamnes et al. developed an OC-SMART algorithm for inversion of aerosol and ocean parameters using nonlinear estimation and the Levenburg–Marquardt method to improve retrieval accuracy [23]. Diner et al. employed nonlinear least squares and retrieved the optical properties and PSD of aerosols through a multi-angle spectrometer [24]. Dubovik et al. retrieved the PSD characteristics of aerosols through light scattering polarization measurements and gave a kernel look-up table [25,26]. Although gradient-based techniques, such as the Levenburg–Marquardt method, are widely used due to maturity and reliability, such algorithms still suffer from cumbersome solutions (requiring complex mathematical calculations) and high dependence on initial values. Specifically, the choice of initial value used for inversion can significantly affect the solution and the accuracy of the results (an ill-posed problem). Hence, researchers have developed various intelligent optimization algorithms to avoid these problems. These intelligent algorithms have the advantages of simple solution and easy implementation. Compared with traditional numerical inversion algorithms using gradient-based techniques, intelligent algorithms have unique advantages in the face of the global optimal and high dimensional problem and no longer rely too much on the initial value and do not require the gradient information of the objective function. For example, He et al. retrieved the PSD of aerosols based on the optimal wavelength selection technique and the fruit fly optimization algorithm [27]. Yuan et al. inverted the PSD characteristics of aerosols through a log normal distribution model and stochastic particle swarm optimization algorithm (SPSO) [28]. Zhang et al. developed a quantum-behaved particle swarm algorithm to invert the PSD and complex refractive index of aerosols [29].

Among the intelligent algorithms, the PSO algorithm has strong global search ability and problem adaptability and has been widely used. However, the basic PSO algorithm has low computational efficiency and easily falls into local optima. Hence, in this paper, an improved stochastic particle swarm optimization (ISPSO) is proposed to invert the PSD characteristics of aerosols based on the advantages of intelligent optimization algorithms. The algorithm optimizes the iterative formula of the traditional particle swarm optimization algorithm and adds random particles to the particle swarm after iteration, which has better global search ability and convergence performance than various traditional intelligent algorithms. Additionally, the robustness of the algorithm is verified by analyzing random errors, changing inversion parameters, and the number of samples. The adaptability of the algorithm to aerosols is verified by inverting the PSD of different aerosol types. Finally, the example of the inversion of aerosol PSD characteristics in Xianghe is presented. Considering the complex distribution and optical properties of aerosols, the study results in this paper can provide help for effectively obtaining atmospheric aerosol parameters. The symbols used in this paper are given in Table 1.

**Table 1.** Symbol, nomenclature, and abbreviations.

Symbol	Explanation
$N$	The number concentration of aerosols for log normal distribution, $\text{cm}^{-3}$
$r_m$	Mean radius for log normal distribution, $\mu\text{m}$
$\sigma$	The standard deviation for log normal distribution
$\tau$	Aerosol optical depth
$r$	Particle radius, $\mu\text{m}$
$\kappa$	Extinction factor of aerosol particle
$m$	Complex refractive index, $n \pm ki$
$\lambda$	Wavelength, $\mu\text{m}$
$n(r)$	The number concentration of aerosols with particle size greater than $r$ , $\text{cm}^{-3}$
$n$	The dimension of the particle swarm
$x$	The position of the particle in the solution space
$v$	The velocity of the particle in the solution space
$i$	The number of iterations
$c_1, c_2$	Acceleration coefficient
$G^d, G^b$	The individual and global best position
$\omega$	Inertia weight for PSO
$\omega'$	Inertia weight for ISPSO
$\zeta_1, \zeta_2, \zeta_3$	The adjustment factor for ISPSO
$\psi$	Control factor for ISPSO
$\gamma$	Random error, %
$\delta$	Relative error, %
$V_m$	The aerosol column volume concentration, $\mu\text{m}^3 \cdot \mu\text{m}^{-2}$

## 2. Materials and Methods

### 2.1. Aerosol Particle Size Distribution and Fredholm Integral Equation

Various size distribution functions have been used to describe the PSD, such as the Weber distribution and log normal distribution, and the log normal distribution has been proved to be accurate and efficient in aerosols (the effect of using the log normal distribution is shown in Figure A1):

$$\frac{dn(r)}{d\ln(r)} = \frac{N}{\ln\sigma\sqrt{2\pi}} \exp\left(-\frac{(\ln r - \ln r_m)^2}{2\ln^2\sigma}\right), \quad (1)$$

where  $N$  is the number concentration,  $r_m$  and  $\sigma$  represent the mean radius and standard deviation, respectively.

The inverse radiation problem of solving PSD is based on the forward radiation problem of calculating aerosol optical depth (AOD). Hence, the Fredholm integral equation of the first kind expressing the relationship between AOD and the columnar aerosol PSD can be written as [30]:

$$\tau = \int_{r_{\min}}^{r_{\max}} \pi r^2 \kappa(r, m, \lambda) \frac{dn(r)}{dr} dr, \quad (2)$$

where  $\tau$  is the AOD;  $\kappa(r, m, \lambda)$  represents the extinction factor of aerosols;  $m$  is the complex refractive index; and  $n(r)$  represents the PSD function of columnar aerosol.

The formula of inversion (objective function) can be obtained by bringing the log normal distribution into the integral equation:

$$\tau_{\text{retrieval}} = \int_{r_{\min}}^{r_{\max}} \pi r^2 \kappa(r, m, \lambda) \frac{N}{\ln\sigma\sqrt{2\pi}} \exp\left(-\frac{(\ln r - \ln r_m)^2}{2\ln^2\sigma}\right) dr, \quad (3)$$

where  $\tau_{\text{retrieval}}$  is the AOD obtained from the inverse problem;  $N$ ,  $r_m$ , and  $\sigma$  are the unknown parameters to be inverted; and the upper and lower limits of the integration can be obtained by the  $3\sigma$  criteria.

## 2.2. Improved Stochastic Particle Swarm Optimization Algorithm

The PSO algorithm is a kind of random search algorithm which belongs to the heuristic algorithm based on the swarm, and its basic idea comes from the imitation of natural laws. The algorithm adopts an information-sharing mechanism, and the core idea can be summarized as: particle swarm searches for the target solution based on group cooperation by simulating the foraging behavior of birds. Each particle moves and updates velocity through the group and its own experience (one iteration). The experience comes from the record of the best position of the group and the particle (the quality of the position is judged by the objective function). This mechanism makes the particle swarm gradually gather to the area where the target is located until the particle finds the target solution (the position of any particle from the target is smaller than the requirement) [31,32].

The particle searches for the target solution in the solution space (the target solution is unknown, and the relative distance of the particle to the solution can be judged by the objective function) and has two properties of position and velocity. If the dimension of the solution space is  $n$  (each dimension corresponds to an unknown parameter in this paper, and the  $N, r_m, \sigma$  constitute a solution, and the variation range of  $N, r_m, \sigma$  constitutes a three-dimensional solution space), the position of the particle is  $x^{(n)} = (x^1, x^2, \dots, x^n)^T$ , and the velocity of the particle is  $v^{(n)} = (v^1, v^2, \dots, v^n)^T$ . The position of any particle in the swarm is randomly initialized by giving upper and lower limits:

$$\xi = rand[0 - 1](\xi_{max} - \xi_{min}) + \xi_{min}, \quad (4)$$

where  $\xi$  is the arbitrary parameter of particles.

The quality of the solution searched by the particle is evaluated by fitness (the quality is inversely proportional to the distance from the target solution). In this paper, the larger the fitness, the better the quality of the solution. Referring to the definition of variance, the fitness of any particles can be expressed according to Equation (3):

$$fitness = 1 / [\sum_{k=1}^n (\tau_{object} - \tau_{inversion})^2 / n], \quad (5)$$

where  $\tau_{object}$  and  $\tau_{inversion}$  are the target AOD and the AOD, respectively, calculated based on Equation (3) through the searched  $N, r_m, \sigma$  in the solution space. The reciprocal means that the greater the fitness, the closer to the target solution. The value  $k$  generally ranges from 1 to 4 and represents the four spectral channels (440 nm, 675 nm, 870 nm, and 1020 nm) often used to invert the PSD.

The movement of particles in the solution space (the update of position and velocity) is achieved by iterative formulas. According to the Refs. [31,32] of Eberhart and Kennedy, the iterative formulas of the PSO algorithm can be expressed as:

$$v_{i+1}^{(n)} = \omega v_i^{(n)} + c_1 \cdot rand[0 - 1] (G_i^{(n)d} - x_i^{(n)}) + c_2 \cdot rand[0 - 1] (G_i^{(n)b} - x_i^{(n)}), \quad (6)$$

$$x_{i+1}^{(n)} = x_i^{(n)} + v_{i+1}^{(n)}, \quad (7)$$

where  $v$  is the velocity of the particle;  $x$  represents the position of the particle;  $n$  is the dimension of the particle;  $i$  represents the number of iterations;  $c_1$  and  $c_2$  are called acceleration coefficients, which represent the cognitive and social parameters, respectively; and  $G^d$  and  $G^b$  are individual and global best positions, respectively. Meanwhile,  $\omega$  represents the inertia weight of the velocity and varies with the number of iterations:

$$\omega(i) = (i_{max} - i) / i_{max} (\omega_{max} - \omega_{min}) + \omega_{min}, \quad (8)$$

where  $\omega_{max}$  and  $\omega_{min}$  represent the maximum and minimum weights, respectively. The weight value gradually decreases with the number of iterations, indicating that the effect of velocity decreases. Referring to the Equations (6)–(8), the particles adjust the velocity during iteration based on the inertia weight, the global optimal position, and the individual

optimal position and change their position according to the velocity. The global optimal position is the best position searched by the swarm (the solution with highest quality of the swarm), while the individual optimal position is the best position searched by the particle itself. Therefore, the movement of the particles is influenced by both the swarm and the particles themselves, that is, the information sharing mechanism and the proportion of influence can be adjusted by  $\omega$ ,  $C_1$ , and  $C_2$ .

The basic particle swarm optimization is often of low computational efficiency. Meanwhile, the aerosol optical properties (especially the extinction factor) calculated based on Mie theory have significant oscillation characteristics, and the changes in the properties with the particle size are non-convex functions. Hence, it is easy to obtain a local optimum solution by using the PSO algorithm. Based on the above reasons, an improved stochastic particle swarm optimization (ISPSO) algorithm is developed in this paper. The convergence ability and the search capability in solution space are considered to the maximum extent to avoid local optima based on the improvement of the PSO algorithm from Refs. [33,34]. The flowchart of the algorithm is shown in Figure 1, and the iterative formula of the ISPSO algorithm is updated as follows:

$$v_{i+1}^{(n)} = \omega' v_i^{(n)} + c \cdot \text{rand}[0-1] \left[ \psi \left( \zeta_1 G_i^{(n)d} + \zeta_2 G_i^{(n)b} + \zeta_3 x_i^{(n)} \right) - 3x_i^{(n)} \right], \quad (9)$$

$$x_{i+1}^{(n)} = x_i^{(n)} + v_{i+1}^{(n)}, \quad (10)$$

where  $c$  is a positive constant and the same as the acceleration coefficient;  $\zeta_1$ ,  $\zeta_2$ ,  $\zeta_3$  are the adjustment factors and their sum is 1, and the relative ratio of  $\zeta_1$  and  $\zeta_2$  affect the relative influence of individual and global best positions; and  $\psi$  represents the control factor, which is used to describe the relative proportion of  $G^d$  and  $G^b$  to  $x_i$ :

$$\psi = (\Psi_{\max} - 3)(i_{\max} - i)/i_{\max} \cdot \text{rand}[0-1] + 3, \quad (11)$$

and the ratio of  $G^d$  and  $G^b$  to  $x_i$  is 1 when  $\psi$  is equal to 3, and the ratio of  $G^d$  and  $G^b$  is higher (lower) when  $\psi$  is greater (less) than 3. The role of  $\psi$  is to give the swarm additional search capability in the early iterations. The value of  $\psi$  gradually tends to 3 after a period of iteration, and the iterative formula tends to the PSO algorithm. The initial value of  $\psi$  can be set to  $3 \pm 0.1$ .

The  $\omega'$  represents the modified inertia weight of velocity. Considering that the velocity of the PSO algorithm has a minimum value,  $G^b$  often fails to meet accuracy requirements. This makes the algorithm converge early and fall into local optima. Hence, the value of  $\omega'_{\min}$  is 0 in this paper, which means that the velocity of the particle is reduced to 0 after the number of iterations exceeds  $i_{\max}$  so as to avoid the above problems. At this point, the motion of the particle is completely driven by the individual and global best positions. The  $\omega'(i)$  is updated as follows:

$$\omega'(i) = \omega'_{\max}(i_{\max} - i)/i_{\max}, \quad (12)$$

The ISPSO algorithm adjusts the velocity of the swarm through  $c$  and adjusts the relative size of  $G^d$ ,  $G^b$  to  $x_i$  through  $\psi$  and  $\zeta_1$ ,  $\zeta_2$ ,  $\zeta_3$ . In addition, a new particle is randomly generated after one iteration based on the existing particle swarm to further improve the global search capability of the ISPSO algorithm (for more detail, please see Refs. [35,36]). The position of this new particle is expressed as  $x_j^{(n)} = (x^1, x^2, \dots, x^n)^T$ , subsequently updated as follows:

$$G^b = \text{argmax}(\text{fitness}(G_i^d), \text{fitness}(G_j^d)), \quad (13)$$

where  $\text{argmax}(\bullet)$  represents the variable in parenthesis that maximizes the objective function in the angle bracket. The  $G^b$  is replaced by the local optimum solution of the new particle if the particle has the largest fitness after repeated comparison with the swarm.

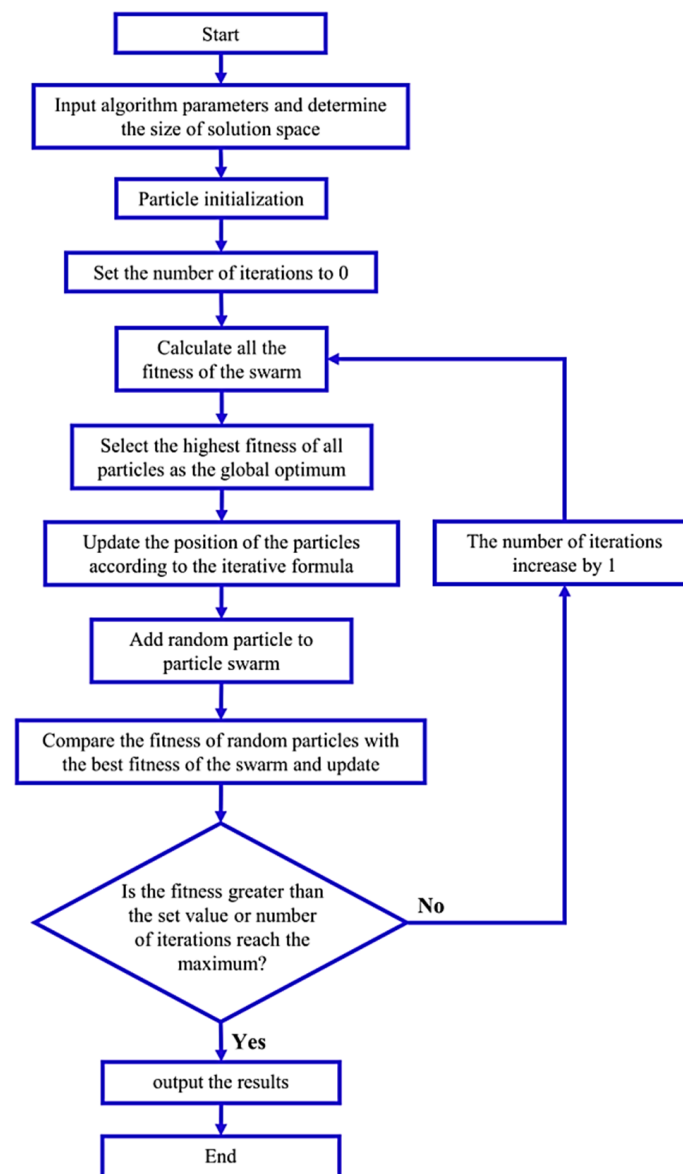


**Figure 1.** The flow of the ISPSO algorithm.

### 3. Results

#### 3.1. The Performance of the Algorithm

In this paper, the performance of the ISPSO algorithm is evaluated by comparing it with traditional intelligent algorithms such as the genetic algorithm (GA) and PSO algorithm. The best fitness variation of different algorithms is shown in Figure 2. The number of maximum iterations is 500. The acceleration coefficients  $c_1$  and  $c_2$  of the standard PSO algorithm are both 1.8, and the inertia weights  $\omega_{max}$  and  $\omega_{min}$  are 0.9 and 0.4, respectively. The basic simulation parameters of the IPSO (improved particle swarm optimization algorithm, no random particles) and ISPSO algorithm are shown in Table 2. The probabilities of mutation and crossover of the genetic algorithm are 0.3 and 0.6, respectively, and the swarm size of all algorithms is 50. The results show that the ISPSO algorithm achieves a higher fitness in a shorter number of iterations compared with the GA, PSO, and IPSO algorithms, so the ISPSO algorithm has higher computational efficiency and better convergence performance.



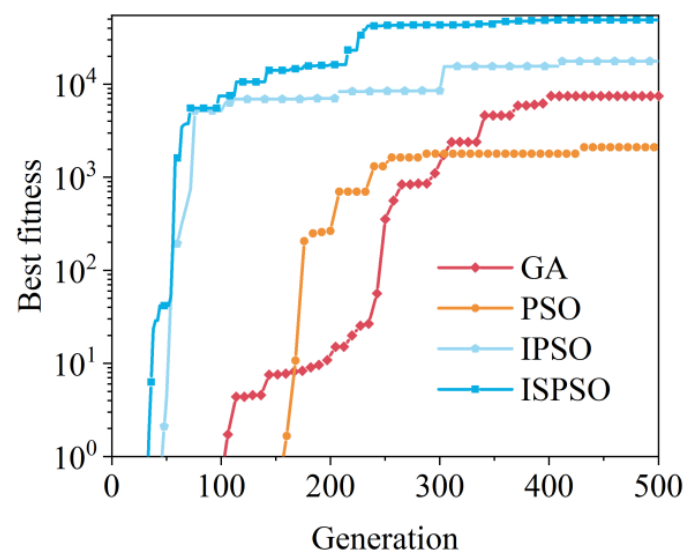


**Figure 2.** The best fitness variation under GA, PSO, IPSO, and ISPSO algorithms.

**Table 2.** The basic simulation parameters of IPSO and ISPSO algorithms.

Swarm Size	Inertia Weight (Maximum) $\omega_{max}$	Inertia Weight (Minimum) $\omega_{min}$	Acceleration Coefficient $c$	Control Factor $\psi$	$\zeta_1$	$\zeta_2$	$\zeta_3$
50	0.9	0	2.0	to 3.0	0.3	0.3	0.4

The inversion of the ISPSO algorithm under different swarm sizes is also compared, and the results are shown in Figures 3 and 4, which are the best fitness and calculation time as a function of the swarm size, respectively. It can be seen that the convergence speed and the fitness of the ISPSO algorithm both increase with the increasing swarm size, but the computation time of the algorithm also increases. The accuracy of the algorithm is not significantly improved when the swarm size of the algorithm exceeds 50. Hence, to take into account both the computational efficiency and computational accuracy, the swarm size is set to 50. In addition, the calculation time of the ISPSO and PSO algorithm is proportional to the swarm size, and the calculation time of the ISPSO algorithm is less than that of the PSO algorithm, which has obvious advantages.

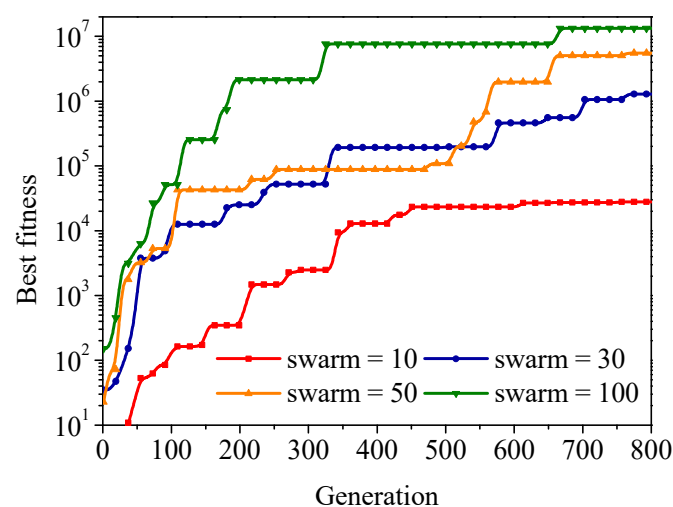


**Figure 3.** The best fitness change of different swarm sizes under the ISPSO algorithm.

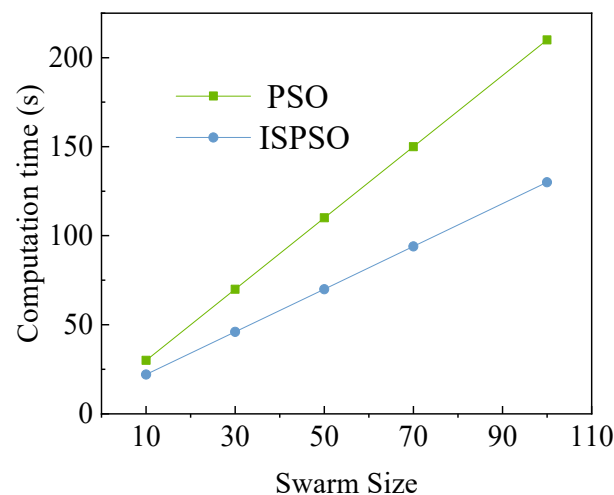


**Figure 4.** Computation time as a function of swarm size under different algorithms.

The mean radius ( $r_m$ ) and standard deviation ( $\sigma$ ) of the ISPSO algorithm and the PSO algorithm for 50-times calculation are shown in Figure 5 (the upper limit of the number of iterations is 500). The inversion results of the ISPSO algorithm are completely concentrated in the neighborhood range of  $(r_m, \sigma) = (1.0, 0.5)$ , so the ISPSO algorithm does not fall into the local optima. However, some of the results of the PSO algorithm fall in another area, which can be considered to fall into the local optima (The distributions of other inversion parameters are shown in Figures A2 and A3).

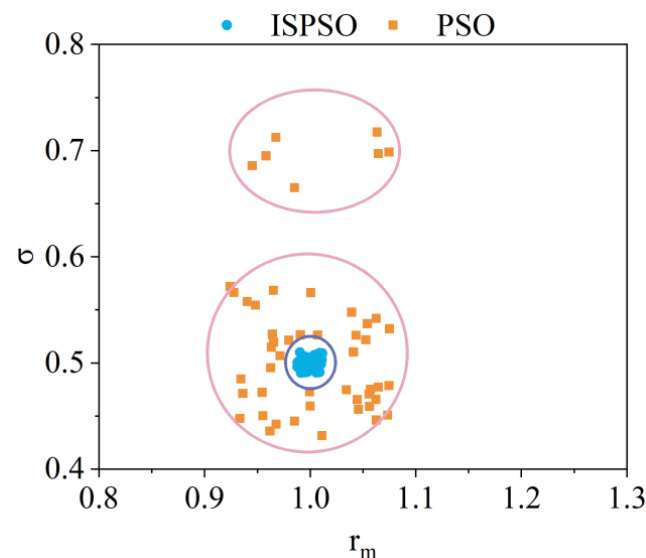


**Figure 5.** The 50-times calculation of ISPSO and PSO algorithms.

### 3.2. Algorithm Verification

In this section, the influence of random error ( $\gamma\%$ ), random initial values, the number of samples, and the number of inversion parameters on the inversion results of the algorithm are analyzed to further verify the robustness of the algorithm (all calculations are repeated 50-times). The relative error  $\delta$  is defined before the simulation:

$$\delta = \left| \frac{P_{true} - P_{calculation}}{P_{calculation}} \right| \times 100\%, \quad (14)$$

where  $P_{true}$  is the true value, and  $P_{calculation}$  is the inversion result. The true value and complex refractive index of inversion are shown in Table 3, including the wavelengths of 250 nm, 440 nm, 675 nm, 870 nm, and 1020 nm.



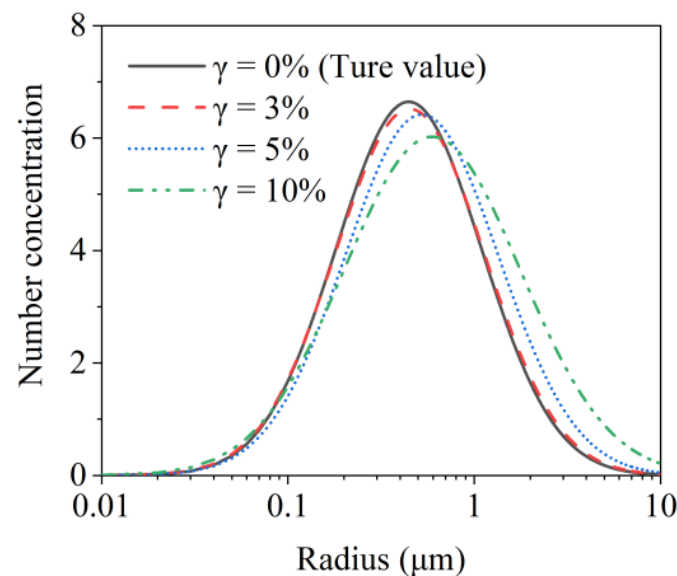
**Table 3.** True value and complex refractive index of different wavelengths.

Wave (nm)	Real Part	Image Part	True Value
250	1.53	0.05	$(N, r_m, \sigma) = (10, 1, 0.9)$
440	1.53	0.008	
675	1.53	0.009	
870	1.52	0.009	
1020	1.50	0.009	

The influence of different random errors ( $\gamma\%$ ) on the algorithm is evaluated, and the results are shown in Table 4. The random errors are 0%, 3%, 5%, and 10%, respectively, and the wavelengths used for inversion are 440 nm, 675 nm, 870 nm, and 1020 nm, respectively. The results show that the inversion value is consistent with the true value when the random error is 0%. As the random error increases, the relative error of the inversion parameters is also rapidly increased. The aerosol PSD characteristics under different random errors are shown in Figure 6. It can be found that the inversion results can still reproduce the real PSD characteristics well when the random error is 3% and 5%, and the relative error with the true value is still acceptable, but the relative error increases sharply when the random error reaches 10% and the inversion result has become unacceptable.

**Table 4.** The relative error under different random errors.

True Value	$\gamma\%$	$N$	$r_m$	$\sigma$	$\delta(N)$	$\delta(r_m)$	$\delta(\sigma)$
$(N, r_m, \sigma) = (10, 1, 0.9)$	0%	10.00	1.00	0.90	0%	0%	0%
	3%	10.34	1.05	0.92	3.40%	5.00%	2.22%
	5%	12.56	1.29	0.95	25.60%	29.00%	5.56%
	10%	17.72	1.95	1.09	77.20%	95.00%	21.11%

**Figure 6.** The PSD characteristics for different random errors.

The relative error of the inversion results of 10 random initial values based on a 5% random error is shown in Figure 7. It can be seen that the relative error does not change significantly with different initial values. The inversion results fluctuate around the average relative error, and the maximum relative error is about 8%. This indicates that the ISPSO algorithm is weakly dependent on the inversion initial value.

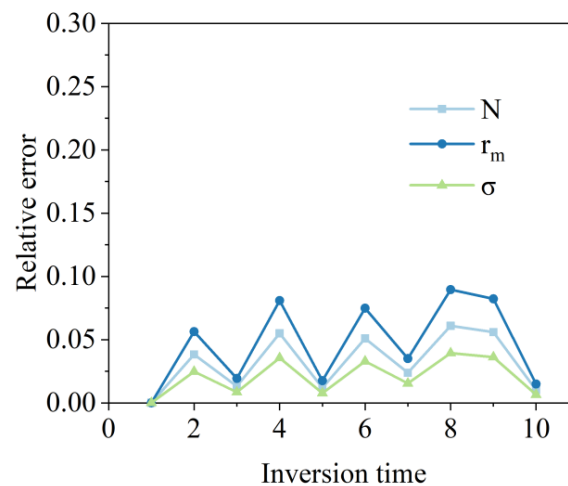


**Figure 7.** The relative error for different random initial values.

The effects of the number of samples on the inversion results are also compared in this paper. The comparison is necessary, because the measurement results of sun photometers in different wavelengths are inevitably noisy and distorted, and severe noise may cause data in a certain wavelength to be unavailable. The results are shown in Table 5 and Figure 8. “Without 440 nm” means that 440 nm is discarded among the four inversion wavelengths of 440 nm, 675 nm, 870 nm, and 1020 nm and uses the remaining three wavelengths for inversion. The other “Without” labels are similar to “Without 440 nm”. “With 250 nm” means that four wavelengths of 250 nm, 675 nm, 870 nm, and 1020 nm are used for inversion. “All wavelengths” means that all five wavelengths are used for inversion. The results show that the inversion results of the two cases such as “All wavelengths” and “With 250 nm” are consistent with the true values, and the relative error is almost 0%. The data of 250 nm successfully replaced 440 nm and played an effective role. However, there is a serious relative error in the inversion results of “Without 440 nm”. As seen in Equations (2) and (3), the more difference between the extinction factor in different wavelengths and the higher the independence between each other, the stronger the resistance to noise (for further analysis, please see Figure A4). Therefore, after removing 440 nm, the remaining three wavelengths are not significantly independent of each other, and the inversion results have a large relative error. However, the relative errors of “Without 675 nm” and “Without 870 nm” are small, indicating that these two wavelengths are less independent of each other. Therefore, if possible, it is easier to obtain accurate inversion results by selecting wavelengths with more independent optical properties.

**Table 5.** The inversion results under different wavelength combinations.

True Value	Type	$N$	$r_m$	$\sigma$	$\delta(N)$	$\delta(r_m)$	$\delta(\sigma)$
$(N, r_m, \sigma) = (10, 1, 0.9)$	With 250 nm	10.01	1.00	0.90	0.10%	0%	0%
	Without 440 nm	18.42	1.95	0.93	84.20%	95.00%	3.33%
	Without 675 nm	10.07	1.01	0.90	0.70%	1.00%	0%
	Without 870 nm	10.11	1.02	0.90	1.10%	2.00%	0%
	Without 1020 nm	14.13	1.29	0.92	41.30%	29.00%	2.22%
	All wavelengths	10.00	1.00	0.90	0%	0%	0%

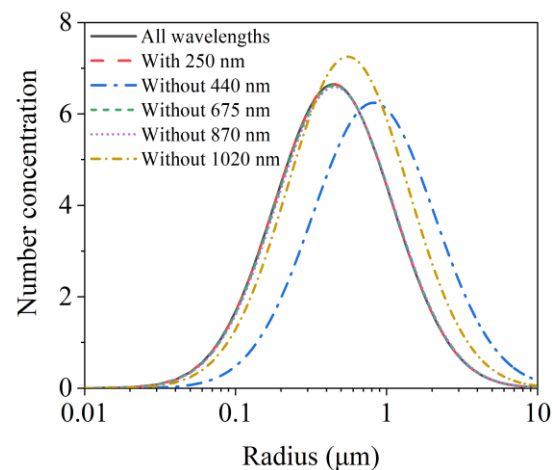


**Figure 8.** The PSD characteristics under different inversion samples.

The influence of the number of inversion parameters is further evaluated in this paper, and the true value of the inversion adopts the double log normal distribution (True value:  $(N_1, r_{m1}, \sigma_1, N_2, r_{m2}, \sigma_2) = (100, 0.2, 0.7, 10, 1, 0.9)$ ). When the number of inversion parameters is 3, then  $N_1$ ,  $N_2$ , and  $r_{m2}$  are unknown, and the rest of the true values are known. When the number of inversion parameters is 4, then  $N_1$ ,  $N_2$ ,  $r_{m1}$ , and  $r_{m2}$  are unknown, and so on. The wavelength and corresponding complex refractive index are shown in Table 3, and the results are shown in Table 6. The results show that the inversion accuracy begins to decrease when the number of inversion parameters is larger than 4. When the number of inversion parameters is 6, the relative error far exceeds 100%, and the inversion results have become unacceptable.

**Table 6.** The relative errors under different numbers of inversion parameters.

True Value	Number of Inversion Parameters	Relative Error
$(N_1, r_{m1}, \sigma_1, N_2, r_{m2}, \sigma_2) = (100, 0.2, 0.7, 10, 1, 0.9)$	3	$\delta(N_1, N_2, r_{m2}) = (0\%, 0\%, 0\%)$
	4	$\delta(N_1, r_{m1}, N_2, r_{m2}) = (11\%, 23\%, 9\%, 21\%)$
	5	$\delta(N_1, r_{m1}, \sigma_1, N_2, r_{m2}) = (93\%, 137\%, 91\%, 87\%, 115\%)$
	6	$\delta(N_1, r_{m1}, \sigma_1, N_2, r_{m2}, \sigma_2) = (152\%, 235\%, 184\%, 136\%, 183\%, 139\%)$

### 3.3. Aerosol Type

To evaluate the adaptability of the ISPSO algorithm to inverse the PSD characteristics of different types of aerosol, three types of aerosol (dust aerosol, water-soluble aerosol, and soot aerosol) are considered. The complex refractive indices at different wavelengths and true values of these aerosols are listed in Table 7 [37,38]. The mean radius of PSD of dust aerosol is much larger than the water-soluble aerosol and soot aerosol. Soot aerosol has the smallest mean radius and the largest complex refractive index (both real and imaginary parts).

**Table 7.** Complex refractive index and true value for three aerosol types.

Wavelength (nm)	440 (n ± ki)	675 (n ± ki)	870 (n ± ki)	1020 (n ± ki)	N	$r_m$	$\sigma$
Dust	$1.52 \pm 0.008i$	$1.52 \pm 0.008i$	$1.52 \pm 0.008i$	$1.52 \pm 0.008i$	10.0	0.54	0.73
Soot	$1.75 \pm 0.46i$	$1.75 \pm 0.43i$	$1.75 \pm 0.43i$	$1.75 \pm 0.43i$	10.0	0.012	0.69
Water-soluble	$1.53 \pm 0.005i$	$1.53 \pm 0.006i$	$1.53 \pm 0.012i$	$1.53 \pm 0.012i$	10.0	0.04	0.80

The inversion results and relative error changes under different random errors and different aerosol types are shown in Table 8 and Figure 9. The results show that the inversion results deteriorate with the increasing random error for any aerosol type, but the

inversion results are generally more reasonable. For dust aerosol and water-soluble aerosol, the accuracy of the inversion results is lower than the soot aerosol under each random error. For soot aerosol, the inversion results vary little with the random error, which indicates that the optical properties of soot aerosol at different wavelengths are more independent and therefore more resistant to noise.

**Table 8.** The inversion results for three aerosol types.

Aerosol	$\gamma\%$	$N$	$r_m$	$\sigma$	$\delta(N)$	$\delta(r_m)$	$\delta(\sigma)$
Dust: ( $N, r_m, \sigma$ ) = (10, 0.54, 0.73)	0%	10.0	0.54	0.73	0%	0%	0%
	3%	10.32	0.59	0.74	3.20%	9.26%	1.37%
	5%	12.13	0.71	0.77	21.30%	31.48%	5.48%
	10%	16.95	1.06	0.85	69.50%	96.30%	16.44%
	0%	10.0	0.012	0.69	0%	0%	0%
Soot: ( $N, r_m, \sigma$ ) = (10, 0.012, 0.69)	3%	10.42	0.012	0.71	4.20%	8.33%	2.90%
	5%	11.41	0.013	0.75	14.10%	8.33%	8.70%
	10%	14.23	0.015	0.87	42.30%	16.67%	26.09%
	0%	10.0	0.04	0.80	0%	0%	0%
	3%	10.27	0.042	0.82	2.70%	5.00%	2.50%
Water-soluble: ( $N, r_m, \sigma$ ) = (10, 0.04, 0.80)	5%	11.89	0.05	0.89	18.90%	25.00%	11.25%
	10%	14.05	0.066	1.01	40.50%	65.00%	26.25%

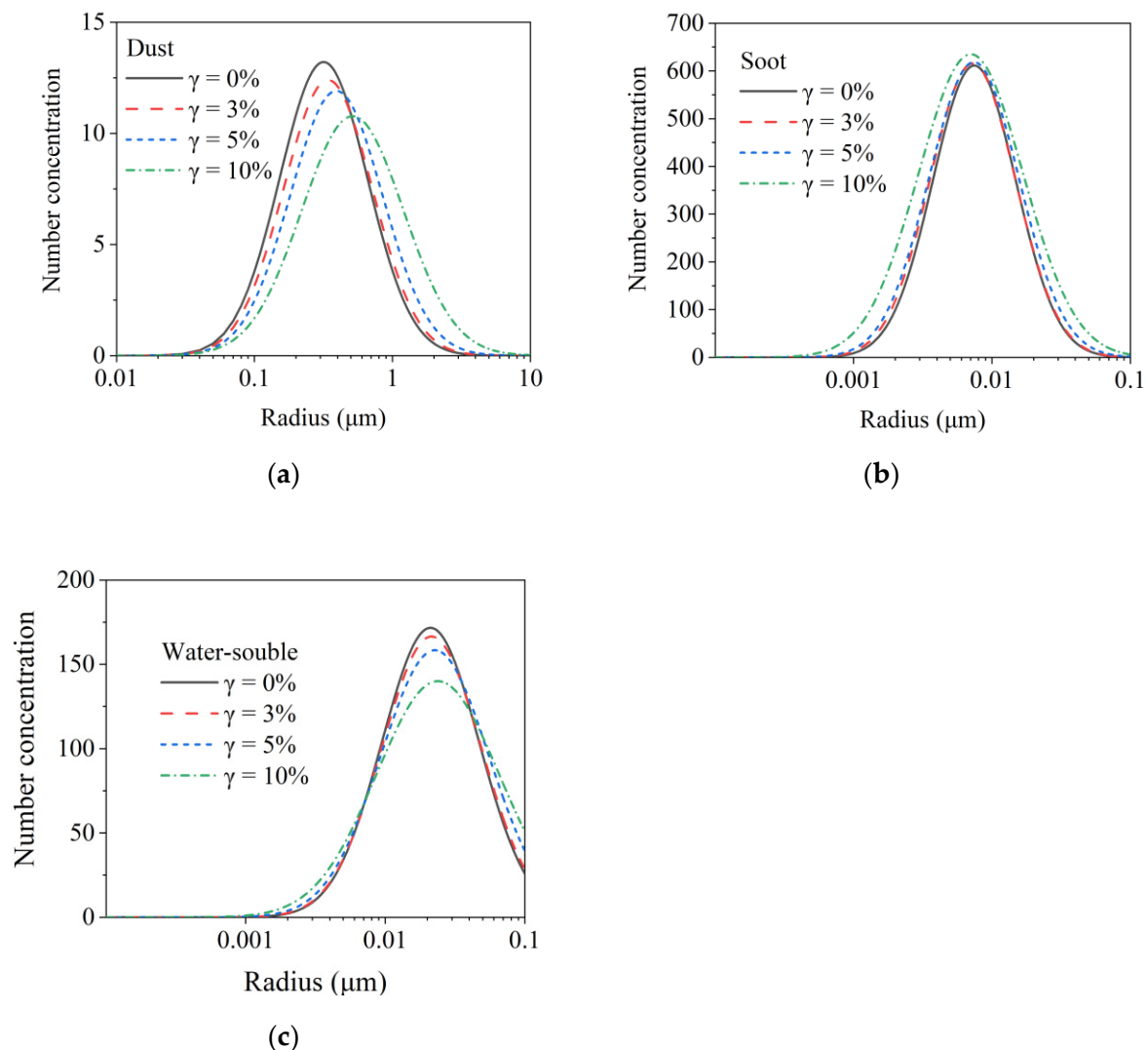


**Figure 9.** The PSD characteristics of the three aerosol types: (a) dust; (b) soot; (c) water-soluble.

### 3.4. Experimental Simulation

Xianghe is densely populated, located in northern China, and prone to dusty weather. Meanwhile, Mezaira is located in the Arabian desert, which is dry and rainy all the year round, and is dominated by dust aerosols. In this paper, the algorithm is verified by two locations with AERONET data. The complex refractive index and PSD are shown in Table 9, and the measurement wavelengths are 440 nm, 675 nm, 870 nm, and 1020 nm, respectively.  $V_m$  is the aerosol column volume concentration, which can be converted to number concentration  $N$  by dividing the sphere volume in the integral term. The sun photometer data from 22 March 2021 and 5 April 2021 (Xianghe) and from 18 July 2018 and 31 July 2018 (Mezaira) are used. The inversion results are shown in Figure 10. The results show that the PSD parameters retrieved by the algorithm are in agreement with the AERONET retrieval products (version 3.0), both in dust and urban aerosols. Hence, the ISPSO algorithm can effectively perform the inversion of aerosol PSD.

**Table 9.** The complex refractive index and PSD measured by AERONET.

Date	Wavelength (nm)	$n \pm ki$	Ture Value ( $V_m, r_m, \sigma$ )
22 March 2021 (Xianghe, dust)	440	$1.6 \pm 0.0032i$	(0.605, 1.716, 0.728)
	675	$1.59 \pm 0.0005i$	
	870	$1.57 \pm 0.0005i$	
	1020	$1.56 \pm 0.0005i$	
5 April 2021 (Xianghe, sunny)	440	$1.47 \pm 0.0059i$	(0.139, 0.339, 1.512)
	675	$1.49 \pm 0.0043i$	
	870	$1.50 \pm 0.0042i$	
	1020	$1.49 \pm 0.0043i$	
18 July 2018 (Mezaira, sample1)	440	$1.53 \pm 0.0022i$	(0.612, 1.230, 1.008)
	675	$1.54 \pm 0.0013i$	
	870	$1.53 \pm 0.0018i$	
	1020	$1.53 \pm 0.0025i$	
31 July 2018 (Mezaira, sample2)	440	$1.52 \pm 0.0023i$	(2.140, 1.243, 0.639)
	675	$1.49 \pm 0.0005i$	
	870	$1.47 \pm 0.0005i$	
	1020	$1.46 \pm 0.0005i$	

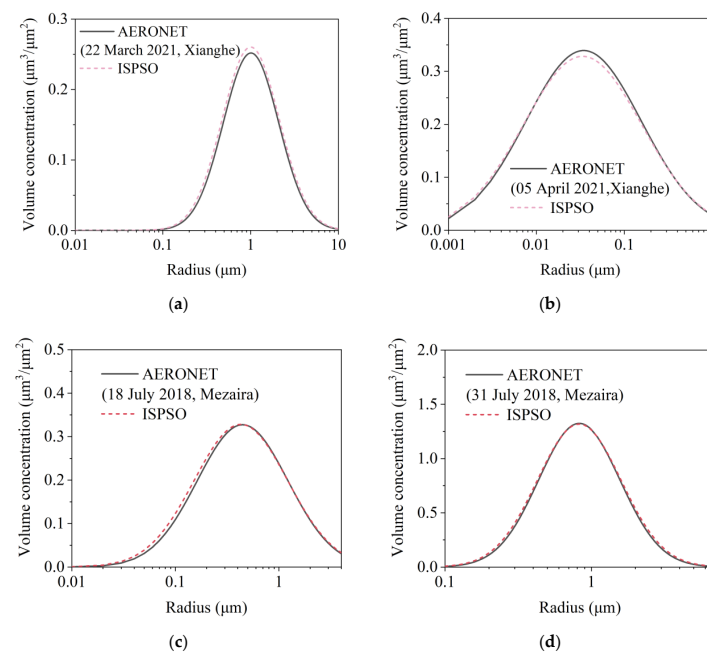


**Figure 10.** The application effect of the algorithm on real case: (a) dusty in Xianghe; (b) sunny in Xianghe; (c) sample1 in Mezaira; (d) sample2 in Mezaira.

## 4. Discussion

### 4.1. The Discussion of Algorithm Performance

The intelligent algorithm is a biologically-inspired method that searches for a target in a solution space by simulating the swarm behavior of organisms. The idea of group collaboration makes this kind of algorithm more suitable for global optimal problems. Especially for the SPSO algorithm with random particles, it seldom falls into the local optima compared with the PSO algorithm [28,33]. The advantages of the PSO algorithm make it easier to be modified and improved. The improved algorithm (ISPSO) undoubtedly has better performance and convergence ability compared with various traditional intelligent algorithms (such as the PSO algorithm and the GA algorithm). Additionally, the optimal swarm size of the intelligent algorithm is affected by the dimension of the solution space, the search range, and the objective function (Equation (3)), but the conditions such as the objective function are not significantly different in some intelligent algorithm studies compared with ours [28,33–35,39], so the optimal swarm size is the same (swarm size = 50).

Furthermore, as mentioned in the introduction, the advantages of intelligent algorithms over traditional numerical algorithm are significant. According to the case in Refs. [38,39], the intelligent algorithm has better convergence (or results). Therefore, in some practical applications such as AERONET and SKYNET (for example, the volume PSD of aerosols is retrieved by combining the aerosol optical depth and scattering phase functions measured by AERONET (composite scattering and extinction measurements) [40,41]), the intelligent algorithms can have higher computational efficiency and less dependence on the initial value (easier to avoid the local optima).

### 4.2. The Discussion of Error and Robustness

Since the objective function is a Fredholm integral equation of the first kind and a priori information is used on the PSD characteristics (giving distribution type), the inversion is a clearly ill-posed problem, i.e., small changes in the aerosol optical data may cause a huge error in the inversion results. Hence, this ill-conditioned characteristic of the inversion make robustness an important criterion for evaluating the algorithm [39]. The results of the error analysis show that the relative error of the inversion result relative to the true value rapidly increase with the increasing random error (data noise). The inversion results have begun to be distorted when the random error is 10%. In the inversion results, the relative error of the standard deviation is the smallest, and the mean radius is the largest. The effect of different inversion parameters on the objective function is different. The bigger the effect of the inversion parameters (the higher the sensitivity), the stronger the ability to resist noise. In addition, the weak dependence on the inversion initial value and the search range are a significant advantage of the intelligent algorithm, and the inversion results of multiple random initial values and subsequent studies verify this advantage.

The number of inversion samples and inversion parameters is also an important factor affecting the uncertainty of inversion. The relative number of inversion samples and parameters makes the calculation indetermined or overdetermined. The overdetermined equation need not be discussed, but for the indetermined problem, the independence between samples becomes very important. The stronger the independence between samples, the higher the ability to resist noise. Hence, the independence between the samples of 675 nm and 870 nm wavelength is weak, so the inversion results are little affected after deleting either of the two samples. Similarly, the relative error of inversion results increases rapidly with the increasing number of inversion parameters.

In summary, when the independence of the samples is insufficient and the number of inversion parameters significantly exceeds the samples, the accuracy of the inversion results will be unacceptable. When dealing with the double log normal distribution or others, the uncertainty of the inversion can be reduced in the following ways: (1) As shown in Table 5 and Figure 8, the ill-posed problem of inversion can be effectively avoided by selecting appropriate data to increase the independence between samples. (2) If the number of inversion parameters is significantly larger than samples, some unknown parameters

can be given a priori. For example, Yuan Yuan et al. used the number concentration only in the log normal distribution as an unknown parameter to obtain the PSD characteristics of aerosols [28]. (3) More samples for inversion can be used; for example, angular light scattering measurements are used to obtain the aerosol PSD and complex refractive index [29].

#### 4.3. The Discussion of Inversion of Aerosol Type

Atmospheric aerosols can be described by the PSD and the complex refractive index when the aerosol is assumed to be spherical. Different aerosols have different PSD and complex refractive index, resulting in different optical properties (such as extinction factor) at a given wavelength. The higher the difference between the aerosol optical property data at different wavelengths, the stronger its independence and thus the stronger the ability to resist noise. Soot aerosol has the best ability to resist noise, while dust aerosol has the worst inversion accuracy from the inversion results. Furthermore, the mean radius had the largest relative error, and the standard deviation had the smallest relative error regardless of aerosol type, which is consistent with the previous analysis.

The data verified by the practical example comes from the Xianghe station, including dust and sunny days. The inversion results agree quite well with the AERONET results. It is easy to obtain consistent results since the AOD data of AERONET comes from the direct inversion of the Beer–Lambert law (have high accuracy) [42]. However, the effect of random errors cannot be ignored when considering the satellite data. The study shows that the measurement error (random error) of AOD may be up to 40% and 20%, respectively, for passive remote sensing such as MODIS and active remote sensing such as Calipso [43–45].

In a future study, the multi-log normal distribution with more inversion parameters will be considered for the ISPSO algorithm, and the atmospheric medium, such as clouds and fog, will also be considered. In addition, the algorithm will attempt to obtain the PSD characteristics of aerosols without being given the distribution type a priori.

## 5. Conclusions

In this paper, the PSD characteristics of aerosols are inverted using the log normal distribution based on the self-developed ISPSO algorithm. The performance evaluation shows that the algorithm has a faster convergence speed and better accuracy than traditional intelligent algorithms. The distribution results of the inversion parameters show that the algorithm can effectively avoid the local optima compared with the PSO algorithm. The ability of the algorithm to resist noise is evaluated by adding random errors of the inversion. Then, the weak dependence of the algorithm on the initial value is reflected through the inversion results of the random initial value. The relative errors of the inversion results of the algorithm under different wavelength combinations and the number of inversion parameters are analyzed, and the applicability and robustness of the algorithm are further clarified. In addition, the study found that the independence of data can significantly affect the accuracy of the inversion results and is proportional to the accuracy. Then, the PSD characteristics of dust aerosol, water-soluble aerosol, and soot aerosol are inverted by the algorithm. The results show that the inversion of three aerosols is reasonable and effective, and the inversion accuracy of soot aerosol is the highest. The results also show that the relative error of the mean radius in the inversion parameters is the largest and the standard deviation is the smallest, which is related to the sensitivity of the inversion parameters in the objective function. Finally, the ISPSO algorithm is used to invert the PSD characteristics of Xianghe and Mezaira combined with AERONET data. The inversion results are in good agreement with the inversion data from AERONET. The ISPSO algorithm is an effective technique to obtain aerosol PSD, and the size distribution can provide support for further study on atmospheric aerosol radiation and environmental effects.



**Author Contributions:** Conceptualization, X.N.; methodology, X.N.; software, X.N.; formal analysis, X.N.; resources, Q.M.; funding acquisition, Q.M.; methodology, X.N.; supervision, Q.M.; validation, Q.M.; writing—original draft preparation, X.N.; writing—review and editing, Q.M. All authors have read and agreed to the published version of the manuscript.

**Funding:** This research was funded by the National Natural Science Foundation of China (No.51876147).

**Data Availability Statement:** The data of this work are freely available from the authors.

**Conflicts of Interest:** The authors declare no conflict of interest.

## Appendix A. The Best Fitness Change for Different Distribution Functions

Atmospheric aerosol is a polydisperse system, and although there are many distribution functions to describe the PSD of atmospheric aerosol, the log normal distribution is the most common. The measured aerosol PSD, complex refractive index, and AOD data from Ref. [39] are used, and the aerosol PSD are assumed to conform to log normal, Weber, and Rosin–Rammler distributions, respectively. The variation of the best fitness with the number of iterations is calculated, and the results are shown in Figure A1. The results show that the log normal distribution has the best convergence performance. Hence, the log normal distribution can best model the PSD of atmospheric aerosols.

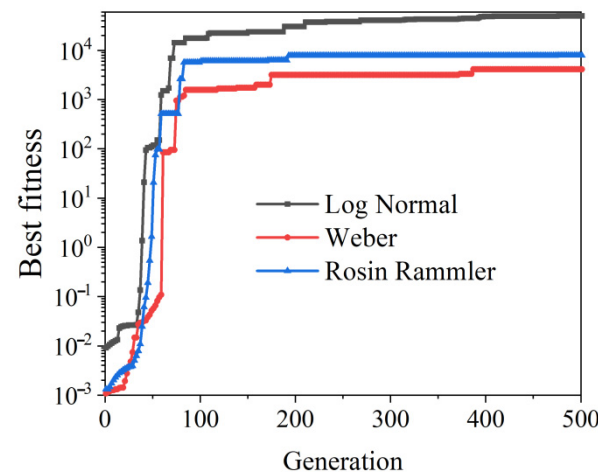


**Figure A1.** The variation of best fitness for different distribution functions.

## Appendix B. The Parameter Distribution of Inversion Results

In addition to the results of  $(r_m, \sigma)$  given in the main text, the results of  $(N, r_m)$  and  $(N, \sigma)$  are also given in Figures A2 and A3 ( $N = 10$ ). The same as the main text, the ISPSO algorithm has no results fall into the local optima, while the PSO algorithm has a small number of inversion results fall into the local optima, which reflects the effectiveness of the random particles.

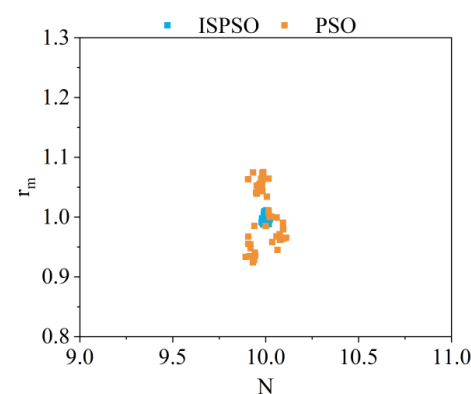


**Figure A2.** The 50-times calculation results of  $(N, r_m)$ .

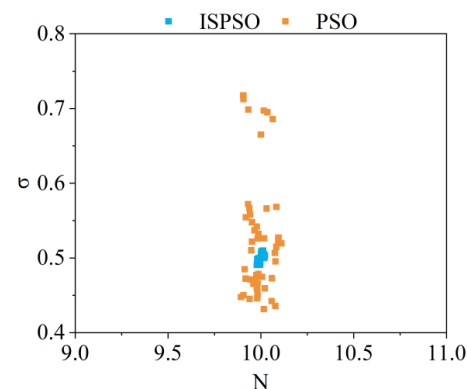


**Figure A3.** The 50-times calculation results of  $(N, \sigma)$ .

### Appendix C. Extinction Factor

According to the parameters given in the main text, the extinction factors at different wavelengths and particle sizes are shown in Figure A4. It can be found that the independence between the wavelengths of 675 nm and 870 nm is not good, far worse than between 440 nm and 1020 nm. Additionally, it can also be found that the extinction factor gradually tends to 2 when the particle size is larger than  $1 \mu\text{m}$ , and the independence of all the wavelengths becomes worse. It can explain why the inversion results of dust aerosol have the largest relative error among the three aerosols simulated in the main text (the effective radius of dust aerosol is greater than  $1 \mu\text{m}$ ).

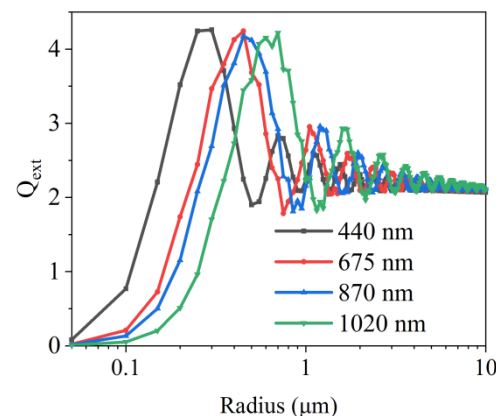


**Figure A4.** The extinction factor as a function of wavelength and particle size.

### References

- Sheng, Z.; Che, H.; Chen, Q.; Xia, X.; Liu, D.; Wang, Z.; Zhao, H.; Gui, K.; Zheng, Y.; Sun, T.; et al. Aerosol vertical distribution and optical properties of different pollution events in Beijing in autumn 2017. *Atmos. Res.* **2019**, *215*, 193–207. [\[CrossRef\]](#)
- Mao, Q.; Nie, X. Polarization performance of a polydisperse aerosol atmosphere based on vector radiative transfer model. *Atmos. Environ.* **2022**, *277*, 119079. [\[CrossRef\]](#)
- Paasonen, P.; Asmi, A.; Petäjä, T.; Kajos, M.K.; Äijälä, M.; Junninen, H.; Holst, T.; Abbatt, J.P.D.; Arneth, A.; Birmili, W.; et al. Warming-induced increase in aerosol number concentration likely to moderate climate change. *Nat. Geosci.* **2013**, *6*, 438–442. [\[CrossRef\]](#)
- Climate Change 2014, Synthesis Report, Summary for Policymakers. Available online: [https://www.ipcc.ch/pdf/assessment-report/ar5/syr/AR5\\_SYR\\_FINAL\\_SPM.pdf](https://www.ipcc.ch/pdf/assessment-report/ar5/syr/AR5_SYR_FINAL_SPM.pdf) (accessed on 21 April 2022).
- Chen, A.; Zhao, C.; Fan, T. Spatio-temporal distribution of aerosol direct radiative forcing over mid-latitude regions in north hemisphere estimated from satellite observations. *Atmos. Res.* **2022**, *266*, 105938. [\[CrossRef\]](#)
- Bellouin, N.; Quaas, J.; Gryspeerdt, E.; Kinne, S.; Stier, P.; Watson-Parris, D.; Boucher, O.; Carslaw, K.S.; Christensen, M.; Daniau, A.L.; et al. Bounding global aerosol radiative forcing of climate change. *Rev. Geophys.* **2020**, *58*, e2019RG000660. [\[CrossRef\]](#)
- Nie, X.; Mao, Q. Study on shortwave radiative transfer characteristics in polydisperse aerosols in a clear sky. *Infrared. Phys. Technol.* **2021**, *118*, 103903. [\[CrossRef\]](#)

8. Xu, F.; Diner, D.J.; Dubovik, O.; Schechner, Y. A correlated multi-pixel inversion approach for aerosol remote sensing. *Remote Sens.* **2019**, *11*, 746. [\[CrossRef\]](#)
9. Mao, Q.; Huang, C.; Zhang, H.; Chen, Q. Aerosol optical properties and radiative effect under different weather conditions in Harbin, China. *Infrared. Phys. Technol.* **2018**, *89*, 304–314. [\[CrossRef\]](#)
10. Si, Y.; Li, S.; Chen, L.; Shang, H.; Wang, L.; Letu, H. Assessment and improvement of MISR Angstrom exponent and single-scattering albedo products using AERONET data in China. *Remote Sens.* **2017**, *9*, 693. [\[CrossRef\]](#)
11. Chen, Q.; Han, X.; Gu, Y.; Yuan, Y.; Jiang, J.H.; Yang, X.; Liou, K.; Tan, H. Evaluation of MODIS, MISR, and VIIRS daily level-3 aerosol optical depth products over land. *Atmos. Res.* **2022**, *265*, 105810. [\[CrossRef\]](#)
12. Fernández-Gálvez, J.; Guerrero-Rascado, J.L.; Molero, F.; Lyamani, H.; Revuelta, M.A.; Navas-Guzmán, F.; Sastre, M.; Bravo-Aranda, J.A.; Fernández, A.J.; Granados-Muñoz, M.J.; et al. Aerosol size distribution from inversion of solar radiances and measured at ground-level during SPALI10 campaign. *Atmos. Res.* **2013**, *127*, 130–140. [\[CrossRef\]](#)
13. Yu, Q.; Zhang, F.; Li, J.; Zhang, J. Analysis of sea-salt aerosol size distributions in radiative transfer. *J. Aerosol. Sci.* **2019**, *129*, 71–86. [\[CrossRef\]](#)
14. Cao, N.; Yang, S.; Cao, S.; Yang, S.; Shen, J. Accuracy calculation for lidar ratio and aerosol size distribution by dual-wavelength lidar. *Appl. Phys. A* **2019**, *125*, 590. [\[CrossRef\]](#)
15. Wang-Li, L.; Cao, Z.; Buser, M.; Whitelock, D.; Parnell, C.B.; Zhang, Y. Techniques for measuring particle size distribution of particulate matter emitted from animal feeding operations. *Atmos. Environ.* **2013**, *66*, 25–32. [\[CrossRef\]](#)
16. Lee, K.; Wong, M.S.; Nichol, J.; Chan, P.W. Retrieval of aerosol size distribution from Microtops II sunphotometer in Hong Kong. *Aerosol. Air. Qualres.* **2015**, *15*, 1712–1719. [\[CrossRef\]](#)
17. He, Z.; Mao, J.; Han, X. Non-parametric estimation of particle size distribution from spectral extinction data with PCA approach. *Powder. Technol.* **2018**, *325*, 510–518. [\[CrossRef\]](#)
18. Wurl, D.; Grainger, R.G.; McDonald, A.J.; Deshler, T. Optimal estimation retrieval of aerosol microphysical properties from SAGE II satellite observations in the volcanically unperturbed lower stratosphere. *Atmos. Chem. Phys.* **2010**, *10*, 4295–4317. [\[CrossRef\]](#)
19. Wang, Y. An efficient gradient method for maximum entropy regularizing retrieval of atmospheric aerosol particle size distribution function. *J. Aerosol. Sci.* **2008**, *39*, 305–322. [\[CrossRef\]](#)
20. Sasi, S.; Natraj, V.; García, V.M.; Efremenko, D.S.; Loyola, D.; Doicu, A. Model Selection in Atmospheric Remote Sensing with an Application to Aerosol Retrieval from DSCOVER/EPIC, Part 1: Theory. *Remote Sens.* **2020**, *12*, 3724. [\[CrossRef\]](#)
21. He, Z.; Liang, D.; Mao, J.; Han, X. Simultaneous estimation of aerosol optical constants and size distribution from angular light-scattering measurement signals. *Chin. Phys. B* **2018**, *27*, 059101. [\[CrossRef\]](#)
22. Kim, H.; Barkey, B.; Paulson, S.E. Real refractive indices of  $\alpha$ - and  $\beta$ -pinene and toluene secondary organic aerosols generated from ozonolysis and photo-oxidation. *J. Geophys. Res.-Atmos.* **2010**, *115*, D24. [\[CrossRef\]](#)
23. Stamnes, K.; Li, W.; Fan, Y.; Hamre, B.; Frette, Ø.; Folkestad, A.; Sorensen, K.; Stamnes, J.J. A new algorithm for simultaneous retrieval of aerosol and marine parameters in coastal environments. *Am. Inst. Phys.* **2013**, *1531*, 919–922.
24. Diner, D.J.; Hodos, R.A.; Davis, A.B.; Garay, M.J.; Martonchik, J.V.; Sanghavi, S.V.; Allmen, P.; Kokhanovsky, A.A.; Zhai, P. An optimization approach for aerosol retrievals using simulated MISR radiances. *Atmos. Res.* **2012**, *116*, 1–14. [\[CrossRef\]](#)
25. Dubovik, O.; Sinyuk, A.; Lapyonok, T.; Holben, B.N.; Mishchenko, M.; Yang, P.; Eck, T.F.; Volten, H.; Muñoz, O.; Veihelmann, B.; et al. Application of spheroid models to account for aerosol particle nonsphericity in remote sensing of desert dust. *J. Geophys. Res.-Atmos.* **2006**, *111*, 1–34. [\[CrossRef\]](#)
26. Smirnov, A.; Holben, B.N.; Eck, T.F.; Dubovik, O.; Slutsker, I. Cloud-screening and quality control algorithms for the AERONET database. *Remote Sens. Environ.* **2000**, *73*, 337–349. [\[CrossRef\]](#)
27. He, Z.; Qi, H.; Yao, Y.; Ruan, L. Inverse estimation of the particle size distribution using the fruit fly optimization algorithm. *Appl. Therm. Eng.* **2015**, *88*, 306–314. [\[CrossRef\]](#)
28. Yuan, Y.; Yi, H.L.; Shuai, Y.; Liu, B.; Tan, H.P. Inverse problem for aerosol particle size distribution using SPSO associated with multi-lognormal distribution model. *Atmos. Environ.* **2011**, *45*, 4892–4897. [\[CrossRef\]](#)
29. Zhang, J.; Qi, H.; Ren, Y.; Sun, J.; Ruan, L. Simultaneous identification of optical constants and PSD of spherical particles by multi-wavelength scattering-transmittance measurement. *Opt. Commun.* **2018**, *413*, 317–328. [\[CrossRef\]](#)
30. Vitale, V.; Tomasi, C.; Lupi, A.; Cacciari, A.; Marani, S. Retrieval of columnar aerosol size distributions and radiative-forcing evaluations from sun-photometric measurements taken during the CLEARCOLUMN (ACE 2) experiment. *Atmos. Environ.* **2000**, *34*, 5095–5105. [\[CrossRef\]](#)
31. Eberhart, R.C.; Kennedy, J. A new optimizer using particle swarm theory. In Proceedings of the Sixth International Symposium on Micro Machine and Human Science, Nagoya, Japan, 4–6 October 1995.
32. Clerc, M.; Kennedy, J. The particle swarm-explosion, stability, and convergence in a multidimensional complex space. *IEEE Trans. Evolut. Comput.* **2002**, *6*, 58–73. [\[CrossRef\]](#)
33. Yuan, Y.; Yi, H.L.; Shuai, Y.; Wang, F.Q.; Tan, H.P. Inverse problem for particle size distributions of atmospheric aerosols using stochastic particle swarm optimization. *J. Quant. Spectrosc. Radiat. Transf.* **2010**, *111*, 2106–2114. [\[CrossRef\]](#)
34. Mao, J.; Li, J. Retrieval of particle size distribution from aerosol optical thickness using an improved particle swarm optimization algorithm. *Opt. Rev.* **2015**, *22*, 809–818. [\[CrossRef\]](#)
35. Qi, H.; Ruan, L.M.; Zhang, H.; Wang, Y.M.; Tan, H.P. Inverse radiation analysis of a one-dimensional participating slab by stochastic particle swarm optimizer algorithm. *Int. J. Therm. Sci.* **2007**, *46*, 649–661. [\[CrossRef\]](#)

36. Wang, Y.; Cheng, Y.; Ji, J.; Zhu, G. Estimation of absorption coefficients for one-dimensional non-uniform medium using particle swarm optimization. In Proceedings of the Second International Symposium on Computational Intelligence and Design, Washington, DC, USA, 12–14 December 2009.
37. Mao, Q.; Huang, C.; Zhang, H.; Chen, Q.; Yuan, Y. Performance of MODIS aerosol products at various timescales and in different pollution conditions over eastern Asia. *Sci. China Technol. Sci.* **2021**, *64*, 774–784. [[CrossRef](#)]
38. Mao, Q.; Cheng, F.; Chen, M. Experimental Study on the Chemical Characterization of Atmospheric Aerosols in Wuhan, China. *Atmosphere* **2021**, *12*, 1393. [[CrossRef](#)]
39. He, Z.; Qi, H.; Chen, Q.; Ruan, L. Retrieval of aerosol size distribution using improved quantum-behaved particle swarm optimization on spectral extinction measurements. *Particuology* **2016**, *28*, 6–14. [[CrossRef](#)]
40. Holben, B.N.; Eck, T.F.; Slutsker, I.; Tanre, D.; Buis, J.P.; Setzer, A.; Vermote, E.; Reagan, J.A.; Kaufman, Y.J.; Nakajima, T.; et al. AERONET-A federated instrument network and data archive for aerosol characterization. *Remote Sens. Environ.* **1998**, *66*, 1–16. [[CrossRef](#)]
41. Sinyuk, A.; Holben, B.N.; Eck, T.F.; Gile, D.M.; Slutsker, I.; Korkin, S.; Schafer, J.S.; Smirnov, A.; Sorokin, M.; Lyapustin, A. The AERONET Version 3 aerosol retrieval algorithm, associated uncertainties and comparisons to Version 2. *Atmos. Meas. Tech.* **2020**, *13*, 3375–3411. [[CrossRef](#)]
42. Hu, F.; Zhang, B.; Chen, Z.; Zhang, X.; Li, J.; Shen, Q.; Tong, Q. Improved algorithm for the retrieval of aerosol optical depth using the sunphotometer CE 318. *Opt. Tech.* **2007**, *33*, 38–41.
43. Singh, R.; Singh, C.; Ojha, S.P.; Kumar, A.S.; Kumar, A.S.K. Development of an improved aerosol product over the Indian subcontinent: Blending model, satellite, and ground-based estimates. *J. Geophys. Res.-Atmos.* **2017**, *122*, 367–390. [[CrossRef](#)]
44. Tao, M.; Wang, Z.; Tao, J.; Chen, L.; Wang, J.; Hou, C.; Wang, L.; Xu, X.; Zhu, H. How do aerosol properties affect the temporal variation of MODIS AOD bias in eastern China? *Remote Sens.* **2017**, *9*, 800. [[CrossRef](#)]
45. Ye, H.; Pan, X.; You, W.; Zhu, X.; Zang, Z.; Wang, D.; Zhang, X.; Hu, Y.; Jin, S. Impact of CALIPSO profile data assimilation on 3-D aerosol improvement in a size-resolved aerosol model. *Atmos. Res.* **2021**, *264*, 105877. [[CrossRef](#)]